

Impact of Modulation Frequencies on the Lifetime of Power Semiconductor Modules for EV Applications

Quentin Gestes¹ and Nicolas Degrenne²

¹ *Ecole normale superieure de Rennes, Bruz, France*
Quentin.Gestes@ens-rennes.fr

² *Mitsubishi Electric R&D Centre Europe (MERCE), Rennes, France*
N.Degrenne@fr.mercede.com

ABSTRACT

Accurate lifetime estimation of power semiconductor modules is necessary in applications such as Electrical Vehicles (EV). This paper presents a new Modulation Frequency (MF) model to estimate the thermo-mechanical cycles caused by drive profiles and motor rotating speed. The paper compares lifetime estimations with conventional Low Frequency (LF) models and shows that when using conventional damage law established by power cycling experiments, the numerous low-amplitude cycles at the modulation frequency play a major role in the degradation of the power semiconductor modules.

1. INTRODUCTION

In Electrical Vehicles (EV), power semiconductor modules condition the electrical energy between the battery and the motor. Because they are subject to wear-out due to thermo-mechanical stress, there is an increasing amount of pressure to predict maintenance intervals and improve replacement costs (Degrenne et al., 2015). In automotive applications, the operating and environmental conditions vary widely and the reliability of the converter is less deterministic. Model-based lifetime estimation methods were developed with a step-wise approach (Hirschmann, Tissen, Schröder & DeDoncker, 2007), (Mainka, Thoben & Schilling, 2011) and (Qiu et al., 2016). The input of the method is an on-line measure or an estimation of the usage (Degrenne & Mollov, 2016). An electromechanical model of the motor and electrical, thermal and damage models of the power semiconductor module are employed. One reason why this type of method is not widely adopted is because a number of assumptions and simplifications affect the accuracy of the lifetime estimation. For instance, in the prior art, only the Low Frequencies ($LF \leq 1\text{Hz}$) corresponding to the speed variations are considered, and the

Quentin Gestes et al. This is an open-access article distributed under the terms of the Creative Commons Attribution 3.0 United States License, which permits unrestricted use, distribution, and reproduction in any medium, provided the original author and source are credited.

Modulation Frequencies proportional to the synchronous motor rotational speed ($MF \geq 1\text{Hz}$) are neglected/filtered. Some models able to reproduce the temperature cycles at the modulation frequency were previously developed but never used to estimate the end of life (Vernica, Ma & Blaabjerg, 2016). Even though the associated thermal cycles are partly filtered by the thermal inertia of the power module, they are so numerous that they may still widely impact the lifetime.

The objective of the paper is to study the impact of modulation frequencies on the lifetime of power semiconductor modules in EV applications. Section 2 presents models to simulate the modulation frequencies, and section 3 provides estimations and analysis of the temperature and damage with a typical drive cycle and EV car with and without the modulation frequencies.

2. ELECTROMECHANICAL MODEL

The following section presents models to simulate the modulation frequency. The objective of those models is to MF losses in power semiconductors from the speed of the car. This modelisation is based on Renault Zoe but can be adapted to other EV.

2.1. Mechanical model

Figure 1 presents input and outputs of the mechanical model, the objective of this model is to convert the speed profile into motor operating point.

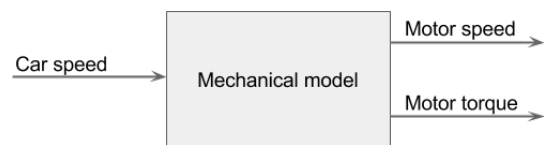


Figure 1. Input and outputs of the mechanical model.

Motor speed is directly derived from car speed using (1) :

$$\Omega = \frac{v}{r} \cdot k \quad (1)$$

where v is car speed ($m \cdot s^{-1}$), r is the radius of the wheel (0.31m) and k is the reduction ratio (9.32).

Figure 2 presents the modelisation of forces applied on the car useful to determine the motor torque.

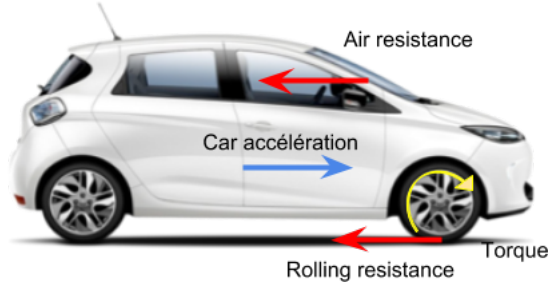


Figure 2. Forces applied on the car

Then the wheel torque is derived using (2):

$$C_r = r \cdot \left(m \cdot \frac{dv}{dt} + m \cdot g \cdot K_r + \frac{1}{2} \cdot \rho \cdot S \cdot C_x \cdot v^2 \right) \quad (2)$$

where m is the mass (1568kg), a is the acceleration ($m \cdot s^{-2}$) derived from the speed v ($m \cdot s^{-1}$), C_x is the drag coefficient (0.338), ρ is the mass density of air ($1.204kg \cdot m^{-3}$), S is the reference area ($2.22m^2$), g is the local acceleration ($9.8N \cdot kg^{-1}$), and K_r is the rolling factor (0.012). Equation (2) assumes that the car is driven on a flat road and that all the parameters are constant.

Finally the motor torque is deduced supposing that transmission efficiency is constant (0.77).

$$C = \frac{C_r}{\eta \cdot k} \quad (3)$$

2.2. Motor model

Figure 3 presents inputs and outputs of the motor model. The objective of this model is to convert the operating point into electrical signals.

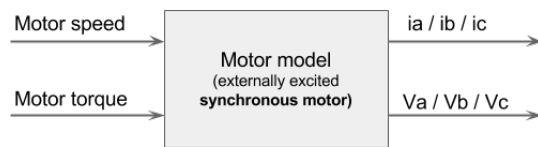


Figure 3. Inputs and outputs of the motor model

This model assumes that the synchronous machine is perfectly self-piloted to zero angle. More precise model with

maximum torque/ampere control for example could be developed to refine the results.

Current and Electromotive force are deduced from equations (4) and (5).

$$\begin{aligned} I_d &= 0 \\ C &= k_\varphi \cdot I_q \end{aligned} \quad (4)$$

$$E = k_\varphi \cdot \Omega \quad (5)$$

where I_d is d-axis stator current, I_q is q-axis stator current, E the electromotive force and (C, Ω) the operating point.

This model also assumes that the magnetic flux is controlled by rotoric current. Figure 4 presents the magnetic flux used in this paper deduced from the operating point.

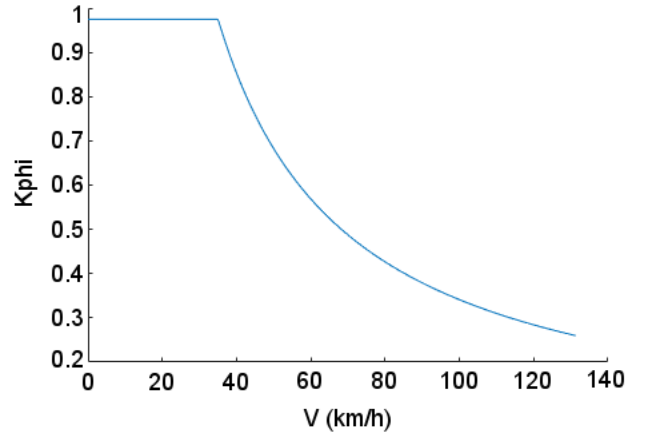


Figure 4. Magnetic flux law

Figure 5 presents the Fresnel diagram of the motor where E is the electromotive force, X_q is q-axis stator inductance (0.2mH), is the self-piloted angle, (I, V) are electrical signals, outputs of the model. The voltage and the angle are then expressed (6). Statoric resistance (0.02Ω) is neglected.

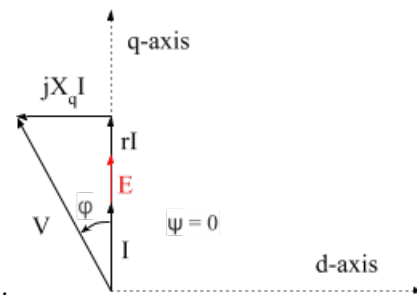


Figure 5. Fresnel diagram of the motor

$$\begin{aligned} V^2 &= E^2 + (X_q \cdot I_q)^2 \\ \tan(\varphi) &= \frac{X_q \cdot I_q}{E} \end{aligned} \quad (6)$$

Finally the electrical signal are obtained using equations (7) and (8).

$$\begin{cases} V_a = V \cdot \sin(p \cdot \Omega \cdot t) \\ V_b = V \cdot \sin(p \cdot \Omega \cdot t - \frac{2 \cdot \pi}{3}) \\ V_c = V \cdot \sin(p \cdot \Omega \cdot t - \frac{4 \cdot \pi}{3}) \end{cases} \quad (7)$$

$$\begin{cases} I_a = I_q \cdot \sin(p \cdot \Omega \cdot t - \varphi) \\ I_b = I_q \cdot \sin(p \cdot \Omega \cdot t - \frac{2 \cdot \pi}{3} - \varphi) \\ I_c = I_q \cdot \sin(p \cdot \Omega \cdot t - \frac{4 \cdot \pi}{3} - \varphi) \end{cases} \quad (8)$$

2.3. Inverter model

Figure 6 presents inputs and outputs of the inverter model. The objective of this model is to convert the electrical signals into semiconductor losses.



Figure 6. Inputs and outputs of the inverter model

This model includes switching and conduction losses. It averages the losses within a switching period. Therefore, the thermal cycles at the switching frequencies ($\leq 10\text{kHz}$) are neglected because they are assumed to be fully filtered by the thermal inertia of the dies. Furthermore this model is based on FP150R07N3E4 module.

The modulation rate is derived from voltage using (9).

$$\alpha = \frac{V}{V_{dc}} + \frac{1}{2} \quad (9)$$

Then losses are expressed by equations (10).

$$\begin{cases} I_{gbt_switching} = F \cdot (E_{on} + E_{off}) \cdot \frac{V_{dc}}{V_{refl}} \cdot \frac{I}{I_{refl}} \\ I_{gbt_conduction} = (V_t + R_t \cdot I) \cdot I \cdot \alpha \\ Diode_switching = F \cdot E_{rec} \cdot \frac{V_{dc}}{V_{refd}} \cdot \frac{I}{I_{refd}} \\ Diode_conduction = (V_d + R_d \cdot I) \cdot I \cdot (1 - \alpha) \end{cases} \quad (10)$$

where V_t , R_t , V_d and R_d represent the constant and current-dependent voltage drop across the IGBT and diode during ON-state. E_{on} , E_{off} and E_{rec} represent energy dissipation. V_{refl} , I_{refl} , V_{refd} and I_{refd} represent the reference constants for loss calculation. F is the switching frequency (10kHz).

Finally figure 7 shows the difference between this MF model and the LF model. In the LF model, steps are due to linearization of the speed. This involves that each second the acceleration and thus the torque and current are constant.

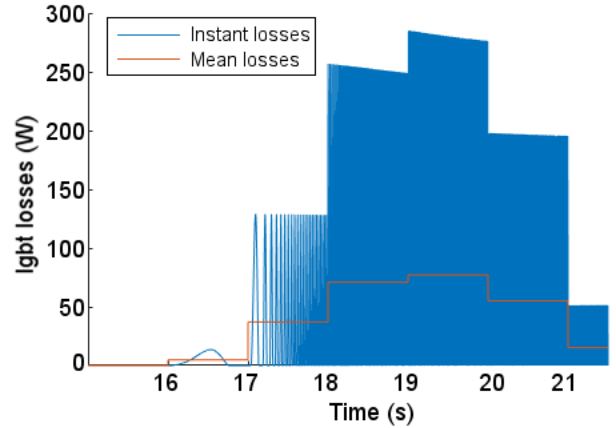


Figure 7. Igbt losses within the MF (instant losses) and LF (mean losses) models

3. DAMAGE ESTIMATION

3.1. Thermal model

Figure 8 presents inputs and output of the thermal model. The objective of this model is to convert semiconductor losses into junction temperature.

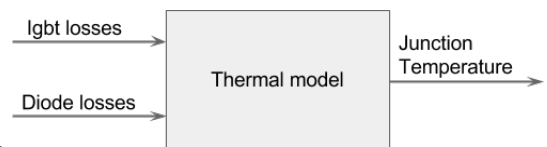


Figure 8. Inputs and output of the thermal model

The Cauer thermal model presented in (Ma et al., 2014) with the values in (Degrenne & Mollov, 2016) was used.

Figure 9 shows that fast thermal cycles are directly linked to losses cycle. There are two important factors for thermal cycle amplitude: the rotational speed and the current. When the first one is high, then the loss variation is fast and filtered by the thermal inertia of the module assembly. Thus, the temperature is quite constant. Finally, the worst situation is at low speed and high torque. A basic strategy could be to limit torque at low speed to increase the reliability of the module.

Figure 10 compares the temperature profiles for the two different models. At low rotational speed, some temperature cycles with amplitude of up to 6°C can be observed at the modulation frequency. When the rotational speed increases, the amplitude of the temperature cycles decreases.

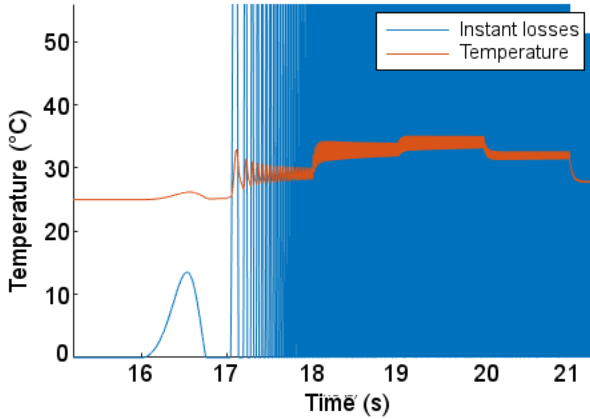


Figure 9. Link between temperature and losses

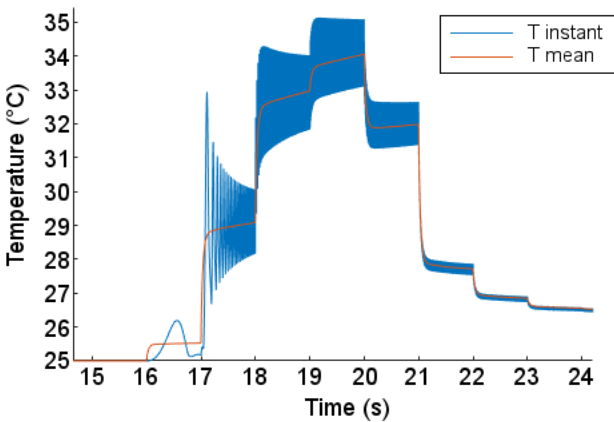


Figure 10. Comparison of the MF and LF models

3.2. Damage model

Figure 11 present input and output of the thermal model. The objective of this model is to convert the junction temperature into damage.

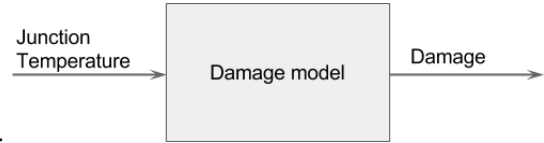


Figure 11. Input and output of the damage model

Thermal cycles are first counted with a rainflow algorithm that returns the number of cycles, the cycle mean temperature and the cycle amplitude.

Figure 12 and 13 shows rainflow algorithm results for each model using DCRA cycle (Degrenne & Mollov, 2016). The calculation confirms the observations made on thermal result showing that the MF model increases the number of fast cycles with low amplitude without influencing high amplitude cycles that are already detected by the LF model.

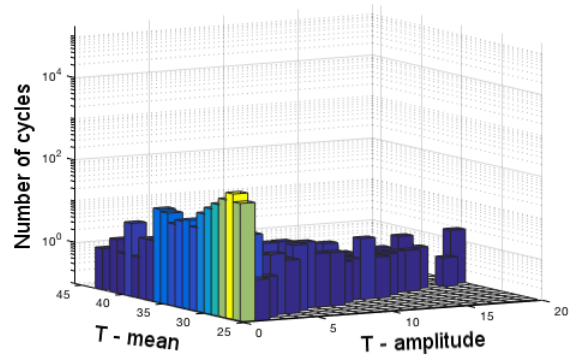


Figure 12. Rainflow result for LF model

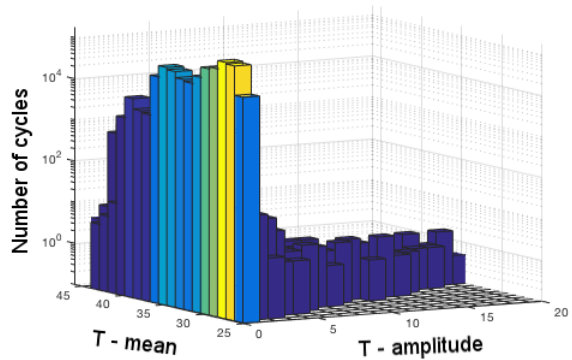


Figure 13. Rainflow result for MF model

Finally, a LESIT law that estimates the number of cycles to failure for cycles with a certain mean and amplitude value was

used with Infineon parameters. Table 1 presents the damage (in %, 100 corresponding to the failure of the power semiconductor module) for each model assuming a linear accumulation law. The MF model increases by a factor of 1000 the estimation of the power semiconductor damage, which means that the lifetime estimation is estimated to be 1000 times lower than with the LF model.

Table 1. Damage result for each model and each semiconductor

Damage	Lf model	Mf model
Igibt	$2.1 * 10^{-9}$	$5.1 * 10^{-6}$
Diode	$5.7 * 10^{-10}$	$1.6 * 10^{-6}$

4. CONCLUSION

In this paper a methodology is presented to estimate the impact of modulation frequencies on semiconductor damage in EV applications. The modulation frequencies results in the generation of a large number of low-amplitude fast thermal cycles. Using a standard damage law, the impact of these cycles on the lifetime is significant. Using a conventional damage law established with power cycling tests at low frequency is certainly not appropriate and results suggest that the damage model should be adapted to model the impact of those low-amplitude and fast cycles.

First, the damage laws are indeed established with temperature cycles of high amplitudes (higher than 60°C). The physical phenomena may be different with low amplitude (elastic versus plastic deformation), making the extrapolation towards low amplitude not simple. In addition, experimental validation is difficult due to the time it would require. Therefore, one solution for the extrapolation to low amplitude is to use Finite Element Simulation thermo-mechanical simulation, for which the material properties needs to be known accurately. Despite the absence of strong scientific proof, the most common belief is that low amplitude cycles in the elastic region have a very low impact on damage. Some recent works show that the impact of small thermal cycles depends on the degradation level of the power semiconductor module (Lai et al., 2016), which also questions the linear damage accumulation hypothesis.

Then, the damage laws are also established with cycles during several seconds. Some power cycling experiments with different temperature swing durations show that the number of cycles to failure tends to increase when the swing duration decreases (Choi et al., 2016) and some damage models were developed to incorporate the swing duration explicitly (Scheuermann, Schmidt & Newman, 2014). For practical use, this type of damage law needs to be calibrated for the automotive power modules and rainflow algorithms measuring pulse length need to be used.

Next, the damage laws are established with tests where losses are created by conduction only. The results may be different in the real situation where the current level to achieve the same temperature is lower because a portion of the losses are switching losses. Switching power cycling tests (Smet, 2010) are being developed and used but are not presently used to generate damage laws. Our research center is developing a switching power cycling test bench for this purpose.

Therefore, some new progresses are required, especially in the definition of damage laws. As a longer term perspective, this type of model-based method can nevertheless be embedded in the car to estimate the remaining useful life of power semiconductor devices in real time, and allow predictive replacement of modules.

5. REFERENCE

- Choi, U. M., Blaabjerg, F., Jørgensen, S., Iannuzzo, F., Wang, H., Uhrenfeldt, C., & Munk-Nielsen, S. (2016). Power cycling test and failure analysis of molded Intelligent Power IGBT Module under different temperature swing durations. *Microelectronics Reliability*.
- Degrenne, N., Ewanchuk, J., David, E., Boldyrjew, R., & Mollov, S. (2007). A Review of Prognostics and Health Management for Power Semiconductor Modules. *PHM society 2015*
- Degrenne, N., & Mollov, S. (2016). Real-life vs . Standard Driving Cycles and Implications on EV Power Electronic Reliability, *IECON 2016*
- Hirschmann, D., Tissen, D., Schröder, S., & De Doncker, R.W. (2007). Reliability prediction for inverters in hybrid electrical vehicles. *IEEE Transactions on Power Electronics*
- Lai, W., Chen, Minyou, Ran, L., Alatisse, O., ; Xu, S., Philip Mawby, P. (2016). Low ΔT_j Stress Cycle Effect in IGBT Power Module Die-Attach Lifetime Modeling, *IEEE Transactions on Power Electronics 2016*.
- Lutz, J., Schlangenotto, H., Scheuermann, U., and De Doncker, R. (2011). *Semiconductor power devices: Physics, characteristics, reliability*. Springer, 2011.
- Ma, K., Yang, Y., & Blaabjerg, F. (2014). Transient modelling of loss and thermal dynamics in power semiconductor devices. *ECCE 2014*.
- Mainka, K., Thoben, M., & Schilling, O. (2011). Lifetime calculation for power modules, application and theory of models and counting methods. *EPE 2011*
- Qiu, Z., Zhang, J., Ning, P., & Wen, X. (2016). Lifetime evaluation of inverter IGBT modules for electric vehicles mission-profile. *ICEMS 2016*.
- Scheuermann, U., Schmidt, R., & Newman, P. (2014). Power

cycling testing with different load pulse durations. PEMD 2014.

Smet, V. (2010). Aging and failure modes of IGBT power modules undergoing power cycling in high temperature environments. Thesis from the University of Montpellier 2.

Vernica, I., Ma, K., & Blaabjerg, F. (2016). Modelling and improvement of thermal cycling in power electronics for motor drive applications. ECCE 2016.